Probing high-energy solar axion flux with a large scintillation neutrino detector

Giuseppe Lucente,[1,2,*] Newton Nath,[2,†] Francesco Capozzi,[3,‡] Maurizio Giannotti,[4,§] and Alessandro Mirizzi[1,2,‖]

[1]*Dipartimento Interateneo di Fisica "Michelangelo Merlin", Via Amendola 173, 70126 Bari, Italy*
[2]*Istituto Nazionale di Fisica Nucleare - Sezione di Bari, Via Orabona 4, 70126 Bari, Italy*
[3]*Dipartimento di Scienze Fisiche e Chimiche, Università degli Studi dell'Aquila, 67100 L'Aquila, Italy*
[4]*Department of Chemistry and Physics, Barry University, 11300 NE 2nd Avenue, Miami Shores, Florida 33161, USA*

(Received 30 September 2022; accepted 17 November 2022; published 8 December 2022)

We investigate the 5.49 MeV solar axions flux produced in the p(d,He3)a reaction and analyze the potential to detect it with the forthcoming large underground neutrino oscillation experiment Jiangmen Underground Neutrino Observatory (JUNO). The JUNO detector could reveal axions through various processes such as Compton and inverse Primakoff conversion, as well as through their decay into two photons or electron-positron pairs inside the detector. We perform a detailed numerical analysis in order to forecast the sensitivity on different combinations of the axion-electron (g_{ae}), axion-photon ($g_{a\gamma}$), and isovector axion-nucleon (g_{3aN}) couplings, using the expected JUNO data for different benchmark values of axion mass in a model-independent way. We find that JUNO would improve by approximately one order of magnitude current bounds by Borexino and it has the best sensitivity among neutrino experiments.

DOI: 10.1103/PhysRevD.106.123007

I. INTRODUCTION

The theory of the strong interactions, quantum chromodynamics (QCD) is expected to violate the charge-conjugation parity (*CP*) symmetry. However, all experimental observations are compatible with *CP* conservation in the strong interactions. Explaining the observed smallness of the *CP* violation in QCD remains, after several decades, an unresolved puzzle in particle physics, known as the *strong CP problem*. The most cogent solution of this problem is to postulate an anomalous global U(1) symmetry—the Peccei-Quinn (PQ) symmetry—that is broken spontaneously, leading to a pseudo-Nambu-Goldstone boson (pNGB) called the QCD axion [1–3]. At the current juncture, the axion is one of the best motivated elementary particles beyond the Standard Model (SM). In fact, in addition to providing the most appealing explanation for the strong *CP* problem, axions are also excellent dark matter candidates [4–11]. The theory allows for many different realizations of QCD axion models, with very specific phenomenology (see Ref. [12] for a comprehensive review).

The model-dependent axion couplings to SM fields open up strategies for their detection. The most accessible experimental detection channels are through the couplings with photons ($g_{a\gamma}$), electrons (g_{ae}), and nucleons (isosinglet g_{0aN} and isotriplet g_{3aN}). These interactions are represented in the effective low-energy axion Lagrangian

$$\mathcal{L} = \frac{1}{2}(\partial_\mu a)^2 - m_a^2 a^2 - \frac{1}{4} g_{a\gamma} a F_{\mu\nu} \tilde{F}^{\mu\nu} - i g_{ae} a \bar{e} \gamma_5 e - i a \bar{N} \gamma_5 (g_{0aN} + \tau_3 g_{3aN}) N, \quad (1)$$

where the first two terms represent the kinetic and mass terms of the axion field a, $F_{\mu\nu}$ and $\tilde{F}^{\mu\nu}$ are the electromagnetic field strength tensor and its dual, and N refers to the proton-neutron isospin doublet.

Typical axion models are constrained to very small masses, below ∼1 eV. However, there exist nonminimal models which predict heavy axions, with masses larger than ∼100 keV, without spoiling the solution of the strong *CP* problem (a list of references can be found in Sec. 6.7 of Ref. [12]). Heavy QCD axions are well motivated since they can provide a simple solution [13] to the axion quality problem [14–19], i.e., the explicit breaking of the $U(1)$ Peccei-Quinn symmetry by higher dimensional

*giuseppe.lucente@ba.infn.it
†newton.nath@ba.infn.it
‡francesco.capozzi@univaq.it
§mgiannotti@barry.edu
‖alessandro.mirizzi@ba.infn.it

Planck-suppressed operators induced by quantum gravity, which could spoil the PQ mechanism. Besides QCD axions, (heavy) axionlike particles (ALPs) emerge in compactification scenarios of string theory [20–22] as well as in "relaxion" models [23]. In this work, we use the term "axions" to refer to both QCD axions and ALPs.

A remarkable experimental effort has been devoted to axion searches in recent years (see Refs. [12,24–28] for recent reviews and updates). Currently, experimental searches have started the exploration of large sections of the parameter space allowed by astrophysical considerations [26,29,30], generating excitement and hopes for discovery in the next decade or so [28,31].[1] Here, our focus will be on studying solar axions. The Sun is one of the most important natural sources of axions. In the hot core, $T_c \sim 1$ keV, axions of mass below a few keV and with thermal energies can be efficiently produced through processes involving the coupling to photons $g_{a\gamma}$, i.e., the Primakoff effect [33,34] and photon-axion conversions in the solar magnetic field [35–37], or the coupling to electrons g_{ae}, such as electrons scattering off nuclei, electron bremsstrahlung and Compton effect [38] (see Ref. [39] for details and updated rates). A stringent constraint on solar axions coupled to photons was placed a few years ago by the CERN Axion Solar Experiment (CAST) [40], which excluded the couplings $g_{a\gamma} > 0.66 \times 10^{-10}$ GeV^{-1} at 95% confidence level for $m_a \lesssim 0.02$ eV. A similar bound can be derived from observations of horizontal branch (HB) stars in globular clusters [41,42]. A more recent analysis [43] found a slightly stronger bound, specifically $g_{a\gamma} \lesssim 0.34 \times 10^{-10}$ GeV^{-1} for $m_a < 1$ keV, by measuring the ratio of stars in the asymptotic giant branch and in the HB in globular clusters.

The very low mass region ($m_a \lesssim$ neV) is subject to considerably more severe constraints from various astrophysical observations (see, e.g., Refs. [44–52]) and is a target for several proposed laboratory searches, e.g., ABRACADABRA [53]. On the other hand, at much larger masses ($m_a \sim$ keV), x-ray observations by NuSTAR [54] have been used to constrain axions trapped in the gravitational potential of the Sun, forming the "Solar basin," leading to very strong bounds on $g_{a\gamma}$ and g_{ae} for $m_a \sim O(10)$ keV [55]. In addition, the flux generated from the axion-electron coupling can be searched by a new generation of axion helioscope experiments, BabyIAXO and IAXO [56,57], which are sensitive to the product of couplings $g_{ae} \times g_{a\gamma}$, and by underground dark matter experiments such as Xenon [58], LUX [59], and PandaX-II [60]. However, the current experimental bounds are not competitive with other astrophysical constraints, in particular with the bounds form red giant stars [61,62]. Finally, the axion couplings with nuclei, g_{0aN} and g_{3aN}, also contribute to the solar axion flux, through nuclear reactions with an axion in the final state, or through deexcitation of nuclei. These are nonthermal processes which produce an almost monocromatic axion spectrum. Since the mass limitation of a few keV for thermal axions does not apply to these processes, they can probe higher masses.

The study of axions from nuclear reactions has a long history, as it was originally considered one of the most efficient way to hunt for these particles [63]. An early attempt to study the axion flux from nuclear processes in the Sun can be found in Ref. [64], and searches for resonant absorption of solar axions emitted in the nuclear magnetic transitions have been performed with ^{57}Fe [65–68], ^{7}Li [69–72] and ^{83}Kr nuclei [73,74]. Recent studies include helioscope sensitivity to different nuclear processes [67,72,75] and a bound on g_{3aN} from SNO data, $g_{3aN} \gtrsim 2 \times 10^{-5}$ (95% confidence level) [76]. Axions from the $p + d \to {}^3\mathrm{He} + \mathrm{a}(5.49\ \mathrm{MeV})$ reaction have been probed by Borexino, constraining the coupling combinations (g_{3aN}, g_{ae}) and $(g_{3aN}, g_{a\gamma})$ [77]. In this work, our goal is to improve the limits set by Borexino using other neutrino experiments. In principle, with respect to [77], Borexino has now collected its full dataset [78], with which most likely the bounds obtained in [77] can be improved. However, an analysis of such dataset is challenging when performed outside of collaboration, especially considering that the detector has been changing significantly over time and the information of this time evolution is not entirely available. Another detector sensitive to MeV neutrinos is Super-Kamiokande [79], whose 22 kton of fiducial mass represents a factor ∼200 improvement with respect to the 100 tons of Borexino. Nevertheless, since we are dealing with the search of monochromatic axions from the Sun, the energy resolution is a key factor, and the better one achieved in Borexino compensates for the relatively low fiducial volume. In terms of future detectors, the proposed Jiangmen Underground Neutrino Observatory (JUNO) represents a step-forward, since it combines a large fiducial mass (∼20 kton) and an exquisite energy resolution $(3\%/\sqrt{E(\mathrm{MeV})}$ [80]. For this reason, in this work, we focus on the JUNO detector, showing that it can improve by about an order of magnitude bounds set by the Borexino. In order to serve our purpose, we consider the JUNO events spectrum provided in Ref. [81]. In particular, we focus on the axion flux from the $p + d \to {}^3\mathrm{He} + \mathrm{a}(5.49\ \mathrm{MeV})$ reaction, as in Ref. [76,77]. This flux can be detected through various processes. The most relevant are the Compton conversion of axions to photons, $\mathrm{a} + e \to e + \gamma$, inverse Primakoff conversion on nuclei, $\mathrm{a} + Z \to \gamma + Z$, axion electron-pair production, and axions decay into two photons as well as two electrons.

We organise the manuscript as follows. In Sec. II we describe the solar axion flux at the source and at the Earth. In Sec. III we discuss how to evaluate the solar axion event rates in JUNO, giving details on the experimental setup and the possible axion interactions in the detector. In Sec. IV we compute JUNO sensitivity, while in Sec. V we compare

[1]Updated plots on axion experimental limits, as well as on other phenomenological bounds, can be found in Ref. [32].

JUNO with other current and future neutrino experiments. Finally, conclusions are summarized in Sec. VI. A discussion of the supernova bound on the axion-nucleon coupling is presented in the Appendix.

II. HIGH-ENERGY SOLAR AXION FLUX

As discussed in the previous section, axions can be nonthermally produced in the Sun through nuclear reaction processes induced by the last term in Eq. (1) (see, e.g., Refs. [82,83] for updated studies). A monochromatic flux of axions is expected to be produced in magnetic dipole transitions from the deexcitation of excited levels of nuclei in the Sun, e.g., $^{57}\mathrm{Fe}^{*} \to {}^{57}\mathrm{Fe} + a(14.4\ \mathrm{keV})$ and $^{83}\mathrm{Kr}^{*} \to {}^{83}\mathrm{Kr} + a(9.4\ \mathrm{keV})$, or from nuclear reactions such as $p + d \to {}^{3}\mathrm{He} + a(5.49\ \mathrm{MeV})$. Detailed studies (see, e.g., Ref. [83] and in particular Fig. 7 therein) show that this last process is one of the most efficient axion production mechanism mediated by the axion-nucleon coupling. This is the *axionic counterpart* of the famous $p + d \to {}^{3}\mathrm{He} + \gamma$ process, responsible for the transformation of nearly all deuterium into ^{3}He nuclei in the Sun. According to the Standard Solar Model, this is the second stage of the pp-solar fusion chain, following the first step in which 99.7% of deuterium is produced after the fusion of two protons, $p + p \to d + e^{+} + \nu_e$, and the remaining 0.3% via the $p + p + e^{-} \to d + \nu_e$ process. Practically, every single deuterium produced in such a way ends up capturing a proton, undergoing the reaction $p + d \to {}^{3}\mathrm{He} + \gamma$ on a timescale of O(1 s). Though this is not the only deuterium reaction allowed in the Sun, the enormous relative abundance of protons with respect to deuterium makes reactions such as $d + d \to p + t$ or $d + d \to n + {}^{3}\mathrm{He}$ extremely unlikely. Consequently, for all practical purposes the standard model predicts one neutrino and one photon for each deuterium nucleus produced in the first stage of the pp chain, $\Phi_{\gamma pp} = \Phi_{\nu pp}$.

If axions exist (and are coupled to nucleons), however, the second stage of the pp chain may produce an axion rather than a photon. The number of axions produced can be related to the number of photons and thus (assuming the axions are not reabsorbed in the solar medium) to the neutrino flux. Specifically, $\Phi_{a0} = (\Gamma_a/\Gamma_\gamma)\Phi_{\nu pp}$, where the coefficient

$$\frac{\Gamma_a}{\Gamma_\gamma} = \left(\frac{k_a}{k_\gamma}\right)^3 \frac{1}{2\pi\alpha} \frac{1}{1+\delta^2} \left[\frac{\beta g_{0aN} + g_{3aN}}{(\mu_0 - \frac{1}{2})\beta + \mu_3 - \eta}\right]^2, \quad (2)$$

measures the probability for a given nuclear transition to result in an axion rather than a photon emission [84]. Here, k_a and k_γ are the axion and photon momenta, α is the electromagnetic fine structure constant, $\mu_0 = \mu_p + \mu_n \approx 0.88$ and $\mu_3 = \mu_p - \mu_n \approx 4.77$ are the isoscalar and isovector nuclear magnetic moments (expressed in nuclear magnetons). The constants δ, β, and η are parameters dependent on the particular nuclear reaction and can be found, e.g., in Ref. [83]. In our specific case, $\beta = 0$, which implies that only the isotriplet axion-nucleon coupling g_{3aN} is relevant in this process. Numerically,

$$\frac{\Gamma_a}{\Gamma_\gamma} \simeq 0.54 g_{3aN}^2 \left(\frac{k_a}{k_\gamma}\right)^3. \quad (3)$$

If axions interact sufficiently weakly, they will escape the Sun without being reabsorbed, just like the neutrinos, and produce an axion flux on Earth. In this case, inserting the known pp solar neutrino flux, $\Phi_{\nu pp} = 6.0 \times 10^{10}\ \mathrm{cm}^{-2}\,\mathrm{s}^{-1}$ [85,86], and accounting for a possible axion decay, we find the expected axion flux on Earth

$$\Phi_a = \Phi_{a0} e^{-d_\odot/l_{\mathrm{tot}}} \simeq 3.23 \times 10^{10} e^{-d_\odot/l_{\mathrm{tot}}} g_{3aN}^2 (k_a/k_\gamma)^3\ \mathrm{cm}^{-2}\,\mathrm{s}^{-1}, \quad (4)$$

where $l_{\mathrm{tot}} = (1/l_\gamma + 1/l_e)^{-1}$ is the total axion decay length, with l_γ and l_e the decay length in photons and electron pairs respectively, and $d_\odot = 1.5 \times 10^{13}$cm the Earth-Sun distance. If the axion interactions are large enough, they can be reabsorbed in the Sun and Eq. (4) becomes invalid. The axion-nucleon coupling can induce axion absorption after the axiodissociation of nuclei $a + Z \to Z_1 + Z_2$. Axions with energy 5.49 MeV can dissociate ^{17}O, ^{13}C and ^{2}H. It is possible to show that couplings $g_{3aN} \lesssim 10^{-3}$ are required for axions not to be trapped inside the Sun [64]. In addition, as discussed in Ref. [77], axions would be trapped in the Sun for $g_{ae} \gtrsim 10^{-6}$ or $g_{a\gamma} \gtrsim 10^{-4}\ \mathrm{GeV}^{-1}$ through inverse Compton and inverse Primakoff absorption respectively (Cf. Sec. III B).

The axion flux from $p + d \to {}^{3}\mathrm{He} + a$ has been explored by the Borexino [77] and by the CAST [40,67,72] experiments via different detection channels related to axion couplings to photons and electrons. Furthermore, using the deuterium "axiodissociation" process $a + d \to n + p$, Ref. [76] derived a bound on g_{3aN} through the analysis of Sudbury Neutrino Observatory (SNO) data, excluding the region $2 \times 10^{-5} < g_{3aN} < 10^{-3}$ [76] for axion masses up to 5.49 MeV. Here, in analogy with Ref. [77], we constrain 5.49 MeV axions detectable in JUNO after interactions with photons and electrons. As we shall see, the axion flux may be large enough to allow the exploration of a region of the parameter space not yet probed by other experiments.

III. JUNO AS A DETECTOR FOR SOLAR AXIONS

In this section, we describe two possibilities of our estimate of the solar axions event rates in JUNO. First, we consider, if axions are detected after interacting with the detector, the expected number of events per unit time is given by

$$N_{\rm ev} = N_T \otimes \Phi_a \otimes \sigma \otimes \mathcal{R} \otimes \varepsilon, \tag{5}$$

where N_T is the number of targets and the initial axion flux Φ_a is convoluted with the cross section σ in the detector, the detector energy resolution $\mathcal{R}$ and the detector efficiency ε. On the other hand, if axions decay into photons or electron-positron pairs inside the detector the event rate is evaluated as[2]

$$N_{\rm ev} = \Phi_a \frac{V}{l_i} \varepsilon, \tag{6}$$

where V is the detector fiducial volume and l_i is the decay length in the ith decay channel. In the following, we assume for all detection channels $\varepsilon = 1$ over the energy threshold.

A. Experimental setup

JUNO is a multipurpose underground liquid scintillator (LS) detector, whose primary physics goal is to determine the neutrino mass ordering (see, e.g., [80] for a review on the detector physics case), thanks to its excellent energy resolution capability and the large fiducial volume.[3] The main features of the JUNO detector have been thoroughly described in Ref. [80]. It consists of a central detector, a water-Cherenkov detector, and a muon tracker. The central detector is a liquid scintillator (LS) of 20 kton fiducial mass with energy resolution

$$\frac{\sigma}{E} = \frac{3\%}{\sqrt{E}}, \tag{7}$$

where both σ and E are expressed in MeV. The detector is made of Linear alkylbenzene (LAB), $C_{19}H_{32}$, doped with 3 g/L of 2,5-diphenyloxazole (PPO) and 15 mg/L of p-bis-(o-methylstyryl)-benzene (bis-MSB). The density of the LS is 0.859 g/ml and it is contained in a spherical container of radius 17.7 m, surrounded by ∼53000 multipliers [80,87].

As discussed in Ref. [81], in order to reduce the background and detect ^{8}B solar neutrinos with a threshold energy of 2 MeV, an energy dependent fiducial volume (FV) cut is considered

(i) FV of 7.9 kton and $r = 13$ m for $2\ \text{MeV} < E \leq 3$ MeV,
(ii) FV of 12.2 kton and $r = 15$ m for $3\ \text{MeV} < E \leq 5$ MeV,
(iii) FV of 16.2 kton and $r = 16.5$ m for $E > 5$ MeV.

Further exclusion cuts to reduce the background are discussed in Ref. [81]. With this experimental set-up and after applying all the cuts about 60,000 solar neutrino events and 30,000 radioactive background events are expected in 10 years of data taking (see Table 4 and Fig. 11 in Ref. [81]). For our work, both types of events contribute to the background. On the other hand, the axion signal induced by the coupling with electrons g_{ae} and photons $g_{a\gamma}$ is produced via the processes discussed in the next section.

B. Axion detection channels

1. Axion-electron coupling

Axions interacting with electrons can be detected through Compton-like scattering $a + e^- \to \gamma + e^-$ [88–90], the axioelectric effect $a + e^- + Ze \to e^- + Ze$ [91–93], pair production in the electric field of nuclei and electrons $a + Ze \to Ze + e^- + e^+$ [94–96], and the decay into electron-positron pairs $a \to e^+ + e^-$.

The integral cross-section for Compton-like scattering σ_C is given by [63,84,97]

$$\sigma_C = \frac{g_{ae}^2 \alpha}{8 m_e^2 k_a} \left[\frac{2m_e^2(m_e + E_a)y}{(m_e^2 + y)^2} + \frac{4m_e(m_a^4 + 2m_a^2 m_e^2 - 4m_e^2 E_a^2)}{y(m_e^2 + y)} + \frac{4m_e^2 k_a^2 + m_a^4}{k_a y} \ln \frac{m_e + E_a + k_a}{m_e + E_a - k_a} \right], \tag{8}$$

where k_a and $E_a = 5.49$ MeV are the momenta and the energy of the axion respectively, m_e is the electron mass and $y = 2m_e E_a + m_a^2$. At fixed value of g_{ae}, the phase space contribution to the cross section is approximately independent of the axion mass for $m_a \lesssim 2$ MeV and the integral cross section reduces to

$$\sigma_C \approx g_{ae}^2 \times 4.3 \times 10^{-25}\ \text{cm}^2. \tag{9}$$

In the axioelectric effect, which is analogue of the photoelectric effect, the axion disappears and an electron is emitted from an atom with an energy equal to the difference between the absorbed-axion energy and the electron binding energy E_b. The cross section for this process is given by

$$\sigma_{ae} = \sigma_{pe} \frac{g_{ae}^2}{\beta} \frac{3E_a^2}{16\pi\alpha m_e^2} \left(1 - \frac{\beta^{2/3}}{3}\right), \tag{10}$$

where $\beta = |\kappa_a|/E_a$ and σ_{pe} is the photoelectric cross section in the medium [98]. As shown in Fig. 1, in JUNO, which is made of LAB ($C_{19}H_{32}$), at energies $\sim O(\text{MeV})$, σ_{pe} is more than 5 orders of magnitude lower than the Compton scattering cross section. Therefore we neglect this latter process in our work. Note, however, that due to the Z^5 dependence of σ_{pe}, the axioelectric effect is

[2]Notice that in this work we consider axions interacting with nucleons and either photons or electrons, but not both. For this reason we are not combining the decay lengths of axions into photons and electrons in Eq. (6).

[3]The JUNO detector can be used to test various new physics predictions, such as proton decay, neutrino nonstandard interactions, and violation of Lorentz invariance.

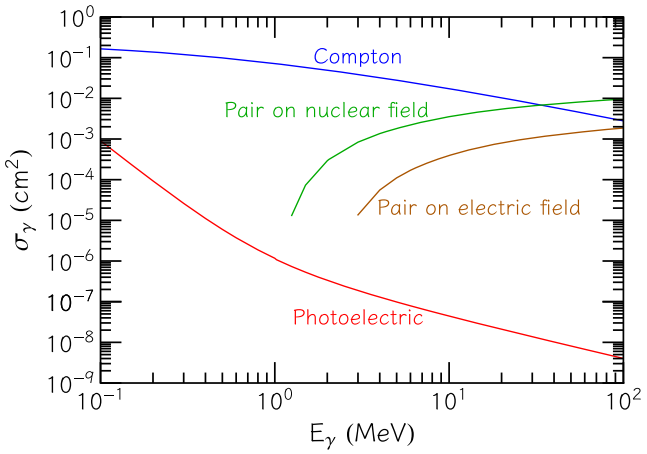

FIG. 1. Cross sections for different photon absorption processes in 1 gram of LAB ($C_{19}H_{32}$). The figure is produced with the XCOM Photon Cross Sections Database [98].

the main axion detection process in detectors with high Z active mass [58–60].

An axion may also produce electron-positron pairs in the electric field of nuclei or electrons. The relevant cross sections for this process were calculated in Refs. [94,95,97,99], soon after the axion was introduced, since this seemed a promising detection channel. Nowadays, the interest in this process has declined. In our case, this process is subdominant with respect to Compton, as reflected in the corresponding photon case shown in Fig. 1. However, we expect this channel to dominate at higher energies and higher values of Z. We ignore this channel in the present work and postpone a detailed analysis of this process to a future project.

Finally, axions with mass $m_a > 2m_e$ can decay into electron-positron pairs, with decay length

$$l_e = \frac{\gamma v}{\Gamma_{a\to e^+e^-}} \simeq 0.33\,\frac{E_a}{m_a}\frac{\sqrt{1-\frac{m_a^2}{E_a^2}}}{\sqrt{1-\frac{4m_e^2}{m_a^2}}}\left(\frac{g_{ae}}{10^{-11}}\right)^{-2}\left(\frac{m_a}{\mathrm{MeV}}\right)^{-1} d_\odot. \quad (11)$$

Therefore, the axion flux arriving on Earth is reduced by a factor $\exp(-d_\odot/l_e)$ as shown in Eq. (4).

2. Axion-photon coupling

Axions coupled with photons can be converted into photons in the electric field of charged particles Ze via the inverse Primakoff effect $a + Ze \to \gamma + Ze$. The differential cross section is given by [100,101]

$$\frac{d\sigma_{\mathrm{P}}}{d\Omega_a} = \frac{g_{a\gamma}^2\alpha}{4\pi}\frac{k_a^4}{q^4}\sin^2\theta_a F^2(q), \quad (12)$$

where θ_a is the scattering angle, $d\Omega_a = d\phi_a d\cos\theta$, and $F(q)$ is the atomic form factor, with $q^2 = m_a^2 - 2E_\gamma(E_a - k_a\cos\theta_a)$ and $E_\gamma \approx E_a$ is the energy of the outgoing photon. We use the following atomic form factor, which includes the electron screening of the nuclear charge [102,103]

$$F^2(q) = Z^2\left[\frac{a^2(Z)|q^2|}{1+a^2(Z)|q^2|}\frac{1}{1+|q^2|/d(A)}\right], \quad (13)$$

where $a(Z) = 111Z^{-1/3}/m_e$ and $d(A) = 0.164\,\mathrm{GeV}^2\,A^{-2/3}$, with A the atomic mass number.

In addition, axions can decay into two photons with decay length

$$l_\gamma = \frac{\gamma v}{\Gamma_{a\to\gamma\gamma}} \simeq 2.64\frac{E_a}{m_a}\sqrt{1-\frac{m_a^2}{E_a^2}}\left(\frac{g_{a\gamma}}{10^{-8}\,\mathrm{GeV}^{-1}}\right)^{-2}\left(\frac{m_a}{\mathrm{MeV}}\right)^{-3} d_\odot. \quad (14)$$

Therefore the axion flux arriving on Earth is reduced by a factor $\exp(-d_\odot/l_\gamma)$ as discussed in Eq. (4). Since the decay rate is proportional to m_a^3, the decay becomes the dominant process for large values of $g_{a\gamma}^2 m_a^3$.

IV. CONSTRAINING AXION COUPLINGS

A. Likelihood analysis

Here, we outline the fitting procedure that we have adopted to characterize the sensitivity of the JUNO detector. JUNO's construction is expected to be completed at the end of 2022 [104]. We estimate the number of events expected to be detected (N_{exp}) using Fig. 11 of Ref. [81], which shows the expected event spectra in ten years of data taking, obtained assuming only SM physics. In order to forecast the detector sensitivity, we define the χ^2 function (see, e.g., Refs. [81,105])

$$\chi^2 = 2\times\sum_i\left(N_{i,\mathrm{pre}} - N_{i,\mathrm{exp}} + N_{i,\mathrm{exp}}\times\log\frac{N_{i,\mathrm{exp}}}{N_{i,\mathrm{pre}}}\right) + \left(\frac{\varepsilon_{\mathrm{sb}}}{\sigma_{\mathrm{sb}}}\right)^2 + \left(\frac{\varepsilon_{\mathrm{rb}}}{\sigma_{\mathrm{rb}}}\right)^2,$$
$$N_{i,\mathrm{pre}} = (1+\varepsilon_{\mathrm{sb}})\times B_{i,\mathrm{sb}} + (1+\varepsilon_{\mathrm{rb}})\times B_{i,\mathrm{rb}} + \frac{S}{\sqrt{2\pi}\bar{\sigma}}\times e^{-\frac{(\bar{E}-E_i)^2}{2\bar{\sigma}^2}}, \quad (15)$$

where $N_{i,\mathrm{exp}}$ is the number of solar neutrino events expected to be observed in the ith energy bin, with energy E_i [81], $N_{i,\mathrm{pre}}$ is the predicted number of events in this energy bin assuming the presence of axions, whereas $B_{i,\mathrm{sb}}$ and $B_{i,\mathrm{rb}}$ represent the solar neutrino and the radioactive background events,[4] taken from Ref. [81]. Here, ε_{sb} and ε_{rb}

[4]We are using $N_{i,\mathrm{exp}} = B_{i,\mathrm{sb}} + B_{i,\mathrm{rb}}$.

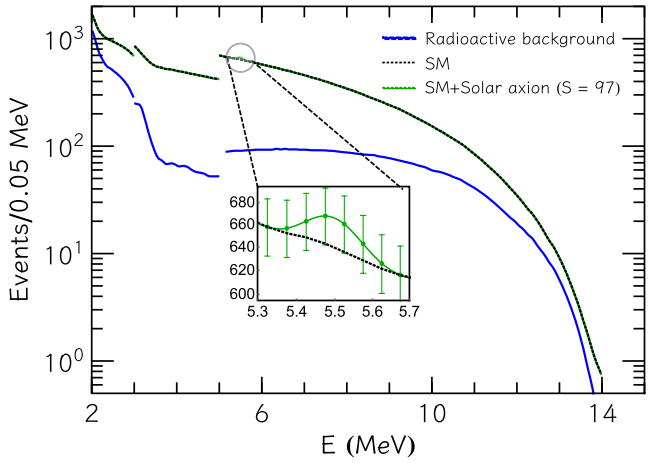

FIG. 2. Expected events spectra for JUNO in 10 years of data taking. The solid blue line represents the radioactive background spectrum. The dotted-black curve shows the standard model (SM) spectrum, obtained summing the expected solar neutrino and the radioactive background events [81]. The solid green curve represents the spectrum expected to be detected in presence of solar axions, with a peak intensity $S = 97$ counts in 10 years, corresponding to the 90% C.L. sensitivity. The inset shows an enlarged picture of the axion induced 5.49 MeV bump. Error bars represent the statistical Poissonian errors.

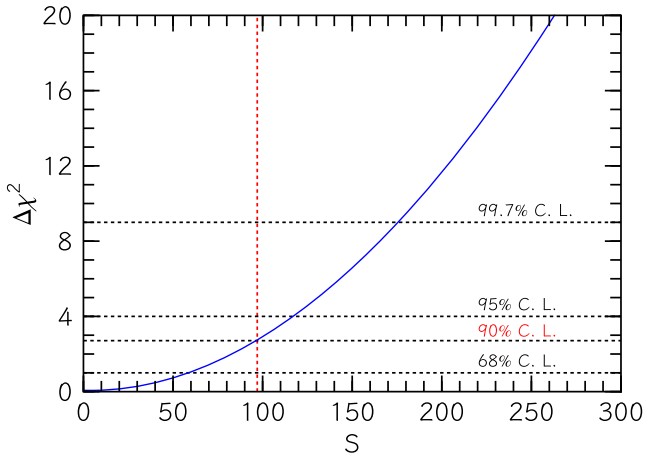

FIG. 3. $\Delta\chi^2$ as a function of the peak intensity S. Here, the horizontal dotted-black lines represent different significance levels. In our analysis, we forecast the sensitivity at 90% C.L., which corresponds to $S_{\rm lim} = 97$, indicated by the vertical dotted-red line.

are the nuisance parameters and the corresponding solar and radioactive background normalization uncertainties are given by σ_{sb} and σ_{rb}, respectively.

The new physics contribution has been modeled as a Gaussian function, with S parametrizing the expected axion peak intensity, centered at $\bar{E} = 5.49$ MeV and with a width $\bar{\sigma} = 0.07$ MeV, given by the detector energy resolution in Eq. (7) evaluated at 5.49 MeV. Figure 2 displays with a dotted black line the total number of expected events from SM in bins with a width of 0.05 MeV, while the blue line represents the contribution from radioactive background only. The breaks in the spectra at 3 and 5 MeV are related to the energy-dependent FV discussed above. On the other hand, the green line shows the total events expected to be detected in presence of solar axions, for a representative value $S = 97$ counts in ten years, corresponding to the 90% confidence level (C.L.) sensitivity, as discussed in the following. The axion bump at 5.49 MeV can be observed.

To perform a χ^2 test, we marginalize over the nuisance parameters and fix the normalization uncertainties for solar and radioactive background as $\sigma_{sb} = 5\%$ and $\sigma_{rb} = 15\%$, respectively. By construction, the χ^2 function is minimized for $S = 0$ (no axion events). A plot of $\Delta\chi^2 = \chi^2(S) - \chi^2_{\rm min}$ as a function of the peak intensity S is shown in Fig. 3. By fixing $\Delta\chi^2(S) = 2.71$, we find that the JUNO sensitivity at 90% C.L.[5] is $S_{\rm lim} = 97$ counts in 10 years. From Eq. (5), this upper limit can be used to constrain the product of the axion flux Φ_a with the cross section of processes having as targets electrons σ_{a-e} or Carbon nuclei σ_{a-C} via [77]

$$S_{\rm events} = \Phi_a \sigma_{a-e,C} N_{e,C} T \varepsilon \leq S_{\rm lim}, \tag{16}$$

where $N_e \simeq 5.5 \times 10^{33}$ and $N_C \simeq 7.1 \times 10^{32}$ are the numbers of electrons and carbon nuclei in the 16.2 kton FV, respectively, $T = 10$ years is the measurement time and $\varepsilon = 1$ is the detection efficiency.[6] Therefore, the individual rate limits at 90% C.L. are

$$\Phi_a \sigma_{a-e} \leq 5.6 \times 10^{-41}\ {\rm s}^{-1}, \tag{17}$$

$$\Phi_a \sigma_{a-C} \leq 4.3 \times 10^{-40}\ {\rm s}^{-1}, \tag{18}$$

almost two order of magnitude smaller than the corresponding Borexino limits [77]. These values describe the sensitivity limit to a model-independent value $\Phi_a \sigma_a$. In this framework, electrons are targets for the Compton effect, while Carbon nuclei for the inverse Primakoff process.

Analogously, in the case of axion decays into photons or electron-positron pairs inside the detector, limits can be obtained by requiring

$$S_{\rm dec} = \Phi_a \frac{V}{l_i} \varepsilon T \leq S_{\rm lim}. \tag{19}$$

To conclude this section, we point out that in general the value of the position $\bar{E}$ and dispersion σ of the Gaussian signal in Eq. (15) could be different for different

[5]We choose to forecast the sensitivity at 90% C.L. to make a direct comparison with Borexino limits [77].

[6]Since we used the fiducial volume, rather than the total volume, the detection efficiency is considered as one.

interactions or decay processes, as discussed by the Borexino collaboration in Ref. [77]. This implies a different value of $S_{\rm lim}$ for each process. In absence of a dedicated Monte Carlo simulation of JUNO response, for simplicity, throughout this work we adopt a unique value of $S_{\rm lim} = 97$ counts in 10 years to serve our purpose. In the next sections, we present our sensitivity study and results derived from the assumptions above.

B. Joint sensitivity on (g_{ae}, g_{3aN})

From Eq. (16), the expected number of events due to Compton conversion in the FV is given by

$$S_C = \Phi_a \sigma_C N_e T, \tag{20}$$

where σ_C is the Compton conversion cross sections in Eq. (8). The axion flux is proportional to g_{3aN}^2 (see Eq. (4), whereas the cross section σ_C for $m_a \lesssim 2$ MeV can be found in Eq. (9). Since $(k_a/k_\gamma)^3 \simeq 1$ for $m_a \lesssim 1$ MeV in Eq. (4), we can simplify Eq. (20) to

$$S_C = g_{3aN}^2 \times g_{ae}^2 \times 2.42 \times 10^{28}. \tag{21}$$

Therefore, at 90% C.L.the sensitivity on the product $|g_{3aN} \times g_{ae}|$ is

$$|g_{3aN} \times g_{ae}| \leq 6.33 \times 10^{-14} \quad \text{for } m_a \lesssim 1 \text{ MeV}. \tag{22}$$

As shown in Fig. 4, this result is one order of magnitude stronger than the Borexino bound $|g_{3aN} \times g_{ae}| \leq 5.5 \times 10^{-13}$ [77] (cyan region). For larger values of the mass, $|g_{a3N} \times g_{ae}|$ depends on m_a due to the kinematic factors in Eqs. (4) and (8).

In addition, for $m_a > 2m_e$ axions can decay into electron-positron pairs. The number of events expected to be detected by JUNO through decay into electron positron pairs is given by

$$S_{e^+e^-} = N_{e^+e^-} T, \tag{23}$$

where

$$N_{e^+e^-} = \Phi_a \frac{V}{l_e}, \tag{24}$$

is the number of $a \to e^+e^-$ decays in the detector, with V indicating JUNO fiducial volume [80] and l_e the decay length in Eq. (11).

Figure 4 shows the parameter space that can be explored by JUNO through the processes mentioned above. At sufficiently small axion-electron coupling ($g_{ae} \lesssim 10^{-11} - 10^{-12}$), we can ignore the reduction in the flux in Eq. (4) due to the $e^{-d_\odot/l_e}$ term. In this case, JUNO would be able to probe the region $|g_{3aN} \times g_{ae}| \sim O(10^{-18})$ for 1 MeV $\lesssim m_a \lesssim 5.5$ MeV. Also in this case, the JUNO sensitivity is an order of magnitude stronger than the Borexino bound.[7]

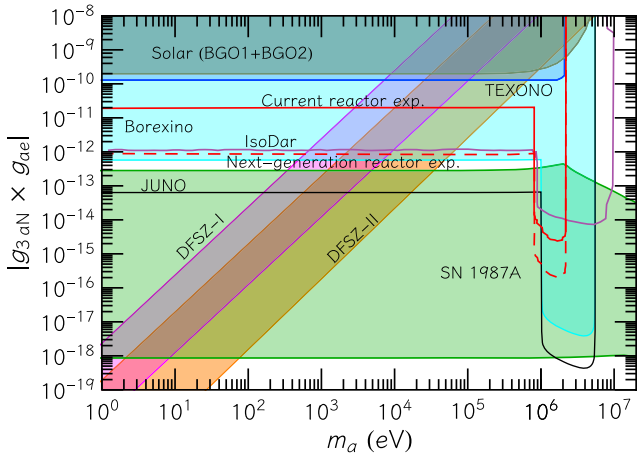

FIG. 4. Exclusion region plot in the $(|g_{3aN} \times g_{ae}|, m_a)$ plane at 90% C.L. The solid black line represents the JUNO sensitivity. Details on the other constraints are given in the main text.

In Fig. 4, we also show other bounds and the sensitivity of future experiments. For $m_a \lesssim 1$ MeV the region $|g_{3aN} \times g_{ae}| \gtrsim 2 \times 10^{-10}$ is excluded at 90% C.L. due to the nonobservation of events induced by solar 5.49 MeV axions through axioelectric effect in $Bi_4Ge_3O_{12}$ (BGO) bolometric detectors [106,107] (see the brown region in Fig. 4). The TEXONO collaboration [108] (blue region) excludes $|g_{3aN} \times g_{ae}| \gtrsim 1.3 \times 10^{-10}$ at 90% C.L. for $m_a \lesssim 10^6$ eV from the nonobservation of axions produced in nuclear transition and detectable after Compton effect in a high-purity germanium detector. Current reactor experiments (solid red line) [109] reach a sensitivity $|g_{3aN} \times g_{ae}| \sim 10^{-11}$, while next-generation experiments (dashed red line) [109] could compete with the Borexino limits. A similar sensitivity (see purple line) will be reached by the Isotope-Decay-at-Rest (IsoDar) experiment, searching for axions using monoenergetic nuclear de-excitation photons from a beam dump [110]. For $m_a < 14.4$ keV, experiments searching for solar ^{57}Fe axions detectable through axioelectric absorption in dark matter detectors using Germanium, such as EDELWEISS III [111], CDEX [112] and MAJORANA DEMONSTRATOR [113], or Xenon targets, such as PANDAX-II [114], constrain the combination $g_{aN}^{\rm eff} = |-1.19 g_{0aN} + g_{3aN}|$. Therefore, assuming $g_{0aN} \approx 0$, these experiments would exclude at most $g_{3aN} \gtrsim 10^{-17}$. These bounds are not shown in Fig. 4 since they cannot be translated univocally into a bound on $|g_{3aN} \times g_{ae}|$. The supernova (SN) bound from the cooling of SN 1987A is the

[7]Notice that the number of axion decays into electron positron pairs was not considered in [77]. For this reason, here we estimate the Borexino bound through Eq. (19) using as benchmark $S_{\rm lim} = 6.9$ counts in 536 days (see Table I in [77]) and the FV of Borexino $\sim 1.15 \times 10^8$ cm^3.

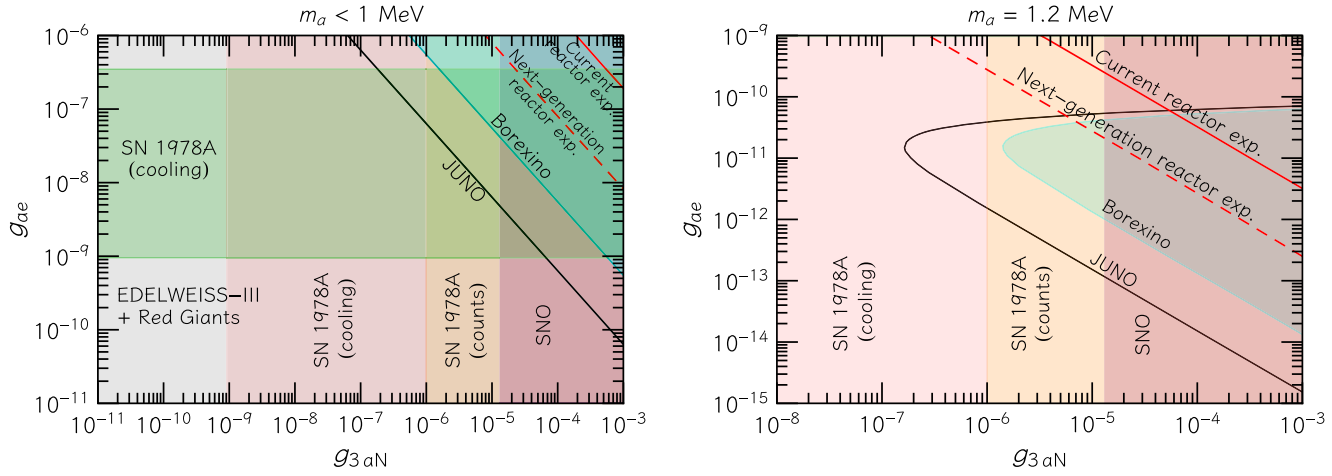

FIG. 5. Left panel: exclusion region plot in the (g_{ae}, g_{3aN}) plane at 90% C.L. for $m_a < 1$ MeV. JUNO sensitivity is shown using the solid black line. Similar bound for Borexino is shown using the solid cyan and colored region. Red lines represent sensitivities of reactor experiments as examined in [109]. Details on the astrophysical bounds are given in the text. Right panel: same as left panel but for $m_a = 1.2$ MeV.

strongest constraint in this region of the parameter space and it is obtained multiplying the values of the constraints on the individual couplings, i.e., $9.1 \times 10^{-10} \lesssim g_{3aN} \lesssim 10^{-6}$ (see Appendix and Ref. [115])[8] and $10^{-9} \lesssim g_{ae} \lesssim 3 \times 10^{-7}$ for $m_a \lesssim 1$ MeV. We observe that JUNO would probe the region of the parameter space for $m_a \lesssim 1$ MeV and $|g_{3aN} \times g_{ae}| \sim 5 \times 10^{-13}$, currently unexplored by direct detection experiments. Finally, we have also displayed the allowed parameter space for the DFSZ-I and DFSZ-II axion models using the light magenta and light orange regions, respectively [109,116,117].

In Fig. 5, we show exclusion region plots in the (g_{ae}, g_{3aN}) plane, at fixed value of the axion mass. In the left panel, the solid black line represents the JUNO sensitivity for axion mass $m_a < 1$ MeV, obtained using Eq. (22). For comparison, we show also bounds arising from the Borexino detector (cyan-colored region) and the sensitivities of current (solid red line) and next-generation neutrino reactor experiments (dashed red line) [109]. It can be noticed that even in this case JUNO has the potential to set constraints on axion couplings that are almost an order of magnitude tighter than those derived from the previous Borexino analysis. However, this region of the parameter space is also constrained by EDELWEISS-III [111] and astrophysical arguments. In particular, the red giant (RG) bound excludes $g_{ae} \gtrsim 1.6 \times 10^{-13}$ [61,62]. In both panels of Fig. 5 we show the SN cooling bound on g_{ae} [118,119] (green region) and g_{3aN} [115] (lighter purple) and constraints arising from additional event counts at Kamiokande-II [120] (lighter orange) and from the SNO analysis [76] (purple). Notice that to express different sensitivities and bounds, we adopts the same color codes throughout the work.

In the right panel of Fig. 5, we show JUNO sensitivity for $m_a = 1.2$ MeV, where the axion decay into electron-positron pairs is relevant. Using Eq. (24) for $m_a = 1.2$ MeV, and T in Eq. (23), limits on the axion couplings for the JUNO detector can be calculated as

$$|g_{3aN} \times g_{ae}| \leq \frac{1.52 \times 10^{-18}}{\sqrt{\exp(-4.25 \times 10^{21} g_{ae}^2)}}. \quad (25)$$

We derive similar limits for the Borexino detector,[9] obtaining

$$|g_{3aN} \times g_{ae}| \leq \frac{1.32 \times 10^{-17}}{\sqrt{\exp(-4.25 \times 10^{21} g_{ae}^2)}}. \quad (26)$$

In this mass range, the sensitivity has a noselike shape, since for couplings smaller than the lower limit not enough axions decay inside the detector, while for values larger than the upper limit, axions decay before reaching the Earth. Also in this case, JUNO is the experiment with the best sensitivity. This region of the parameter space is not constrained by red giants, since the axion production is Boltzmann suppressed for $m_a \gtrsim O(10)$ keV. Thus, the only competitive bound in this region is the SN limit.

[8]We remark that there exist a stronger upper limit on g_{3aN}, specifically $g_{3aN} \lesssim 10^{-5}$, from the analysis of the event counts at Kamiokande-II [120]. However, this argument cannot be applied to constrain g_{ae}. Thus, in Fig. 4 we show only the SN 1987A cooling bound on both g_{ae} and g_{3aN}.

[9]Events from axion decays into electron-positron pairs were neglected in Ref. [77].

C. Joint sensitivity on g_{3aN}, $g_{a\gamma}$

Axion coupled to photons may be detected in JUNO through the Primakoff process or through axion decay into two photons. The JUNO sensitivity in this case is shown in Fig. 6.

The number of expected events due to inverse Primakoff conversion is given by

$$S_P = \Phi_a \sigma_P N_C T \varepsilon_P, \tag{27}$$

where N_C is the number of Carbon nuclei in the FV and σ_P is the Primakoff conversion cross section obtained integrating Eq. (12) over the scattering angle. In the small mass limit ($m_a \lesssim 10$ keV) and under the assumption that $\Phi_a = \Phi_{a0}$ (i.e., $m_a^2(\mathrm{eV}) \times g_{a\gamma}(\mathrm{GeV}^{-1}) < 1.2 \times 10^4$ eV^2 GeV^{-1}), the JUNO sensitivity reaches at 90% C.L.

$$|g_{3aN} \times g_{a\gamma}| \lesssim 6.5 \times 10^{-12}\ \mathrm{GeV}^{-1} \quad \text{for } m_a \lesssim 10\,\mathrm{keV}, \tag{28}$$

improving on the Borexino limits [77] by almost one order of magnitude, as shown in Fig. 6. For larger values of the mass, the axion decay becomes important and the sensitivity on $|g_{3aN} \times g_{a\gamma}|$ depends on m_a. Indeed, the number of events expected to be detected by JUNO after axion decays into two photons is given by

$$S_{2\gamma} = N_\gamma T, \tag{29}$$

where T is the exposure time and N_γ is the number of decays inside the detector

$$N_\gamma = \Phi_a \frac{V}{l_\gamma}, \tag{30}$$

with Φ_a in Eq. (4) and l_γ in Eq. (14). Assuming ultrarelativistic axions, $\beta \sim 1$, the axion decay implies a limit at 90% C.L.

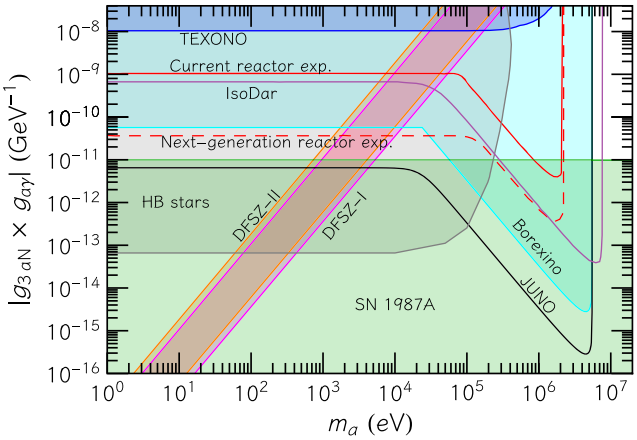

FIG. 6. Exclusion region plot in the ($|g_{3aN} \times g_{a\gamma}|$, m_a) plane at 90% C.L. The solid black line represents JUNO sensitivity. Details on the other constraints and sensitivities are given in the main text.

$$|g_{3aN} \times g_{a\gamma}| \times m_a^2 \lesssim 3.3 \times 10^{-12}\ \mathrm{eV}, \tag{31}$$

for 10 keV $\lesssim m_a <$ 5 MeV, as shown in Fig. 6. In this case, JUNO is capable of exploring axion couplings $|g_{3aN} \times g_{a\gamma}| \sim \mathcal{O}(10^{-15})$ GeV^{-1} for $m_a \sim \mathcal{O}$(MeV). For axion masses closer to the limit of 5.49 MeV, the dependence of the bound on the axion mass changes since the ultrarelativistic assumption for the axions becomes invalid.

For comparison, in Fig. 6 we show also the Borexino bound (cyan) as well as sensitivities of the current (next-generation) neutrino reactor experiments [109] in solid (dashed) red lines and of the IsoDar experiment [110] in purple. Furthermore, we show the TEXONO bound [108] (blue region), constraining $|g_{3aN} \times g_{a\gamma}| \lesssim 7.7 \times 10^{-9}$ GeV^{-1} at 90% C.L. for $m_a \lesssim 10^5$ eV from the nonobservation of axions produced in nuclear transition and detectable after Primakoff conversion in the detector. Finally, we show astrophysical bounds from HB stars and from SN. The SN 1987A bound (green region) is obtained from the constraints on the individual couplings $9.1 \times 10^{-10} \lesssim g_{3aN} \lesssim 10^{-6}$ [115] and 7×10^{-9} GeV$^{-1} \lesssim g_{a\gamma} \lesssim 2 \times 10^{-6}$ GeV^{-1} for $m_a \lesssim 10$ MeV [121].[10] The gray region represents the bound from horizontal-branch (HB) stars in globular clusters [122,123]. Since there is not a HB bound on g_{3aN}, we estimate the constraint on the product $|g_{3aN} \times g_{a\gamma}|$ by requiring that $g_{3aN} \lesssim 10^{-3}$, to allow axions to escape from the Sun. Our analysis shows that, even for the $|g_{3aN} \times g_{a\gamma}|$ combination of couplings, JUNO has the best experimental sensitivity for all the axion masses, improving on the Borexino limit by approximately one order of magnitude. Thus, JUNO has the potential of exploring regions of the axion parameter space currently accessible only through astrophysical arguments.

Finally, in Fig. 7 we show the sensitivity in the ($g_{a\gamma}$, g_{3aN}) plane at fixed values of the axion mass. In the left panel, we show the small mass limit case $m_a < 10$ keV, where the dominant process is the inverse Primakoff, and in the right panel we show the case of $m_a = 1.2$ MeV, where the dominant process is the axion decay. In the small mass limit, the bound follows Eq. (31) and it improves on all the other experimental bounds and sensitivities. This region is constrained by the SN limits previously discussed and the HB bound [41,42] on $g_{a\gamma}$, which completely excludes the experimental region of interest in this mass range. On the other hand, at $m_a = 1.2$ MeV the JUNO sensitivity has the typical noselike shape discussed in the previous section and can probe $g_{a\gamma} \sim 10^{-12}$ GeV^{-1} for $g_{3aN} \sim 10^{-3}$. This region is not constrained by the HB bound, since the

[10]The SN 1987A upper limit on the combination $|g_{3aN} \times g_{a\gamma}|$ could be strengthened by accounting for the event counts bound at Kamiokande-II [120] and from the recent SN bound from energy deposition $g_{a\gamma} \lesssim 5 \times 10^{-5}$ GeV^{-1} for $m_a \lesssim 10$ MeV [121].

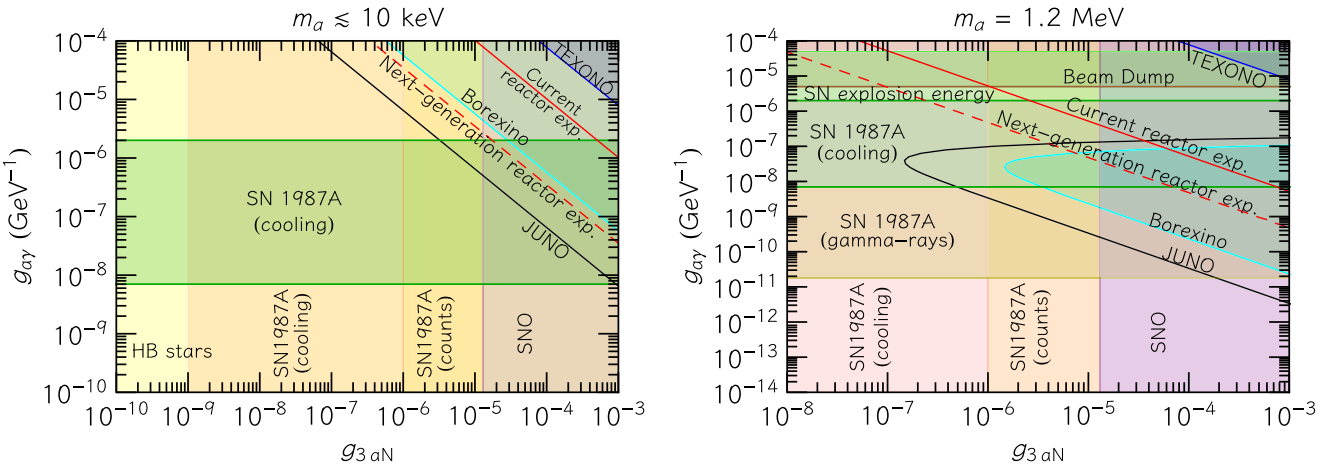

FIG. 7. Left panel: exclusion region plot in the ($g_{a\gamma}$, g_{3aN}) plane at 90% C.L. for $m_a \lesssim 10$ keV. JUNO sensitivity is shown using the solid black line. The solid cyan region is the Borexino bound. Red lines represent sensitivities of reactor experiments as examined in [109]. Details on the other experimental and astrophysical bounds are given in the text. Right panel: same as left panel but for $m_a = 1.2$ MeV.

axion production is suppressed for $m_a \gtrsim O(100)$ keV. There are, however, other astrophysical and experimental limits. Besides the bounds discussed above, in this mass range the couplings $g_{a\gamma} \gtrsim 5 \times 10^{-6}$ GeV^{-1} are excluded by beam dump experiments (brown) [26,124,125], while lower values of the coupling are constrained by requiring that axion decays must not lead to an excessive SN explosion energy (light green) [126] and from the non-observation of a gamma-ray flux in association with the SN 1987A explosion (darker yellow) [121,127].

V. COMPARISON WITH FUTURE NEUTRINO EXPERIMENTS

In this section we evaluate the sensitivity of other forthcoming neutrino experiments to detect 5.49 MeV solar axions. The next-generation Hyper-Kamiokande (HK) neutrino observatory is planned to be installed near Kamioka, in Japan, and is expected to start in 2027 [128]. The HK collaboration plans to use a water-Cherenkov detector with 374 kton fiducial volume with energy resolution

$$\sigma/\mathrm{MeV} = 0.6\sqrt{E/\mathrm{MeV}}. \tag{32}$$

To derive the HK sensitivity on axion couplings, here we adopt the same procedure described in Sec. IV A. We have first calculated the expected solar neutrino events ($N_{i,\mathrm{exp}}$) for the HK detector.

We compute the expected number of neutrinos for the i^{th} energy bin as

$$N_{i,\mathrm{exp}} = \int_{E_i}^{E_{i+1}} \frac{dN_{\mathrm{exp}}}{dE_{\mathrm{vis}}} dE_{\mathrm{vis}}, \tag{33}$$

where,

$$\frac{dN_{\mathrm{exp}}}{dE_{\mathrm{vis}}} = N_e T \varepsilon \theta(E_{\mathrm{vis}} - E_T) \int dT_e \mathcal{R}(E_{\mathrm{vis}}, T_e) \times \int dE_\nu \frac{d\Phi_{\mathrm{sol}}}{dE_\nu} \frac{d\sigma}{dT_e}(E_\nu, T_e), \tag{34}$$

and $\theta(E_{\mathrm{vis}} - E_T)$ is the Heaviside step function. Here, $N_e \simeq 1.5 \times 10^{35}$ represents the number of electrons corresponding to 374 kton detector, T is the 10-year run-time [128], while the detection efficiency $\varepsilon = 1$ has been adopted for the HK detector. Also, E_ν is the neutrino energy, T_e is the kinetic energy of the recoil electron, and $E_T = 3.5$ MeV [129] is the threshold energy necessary to produce an electron. $\mathcal{R}$ is the Gaussian energy resolution function, having a width given by Eq. (32). Using the solar neutrino flux in Ref. [130] and the differential cross sections for the neutrino-electron elastic scattering processes in Ref. [131], Eq. (33) predicts $\sim 3 \times 10^7$ events in the HK detector. Here, we have only considered the solar background normalization uncertainties, $\sigma_{\mathrm{sb}} = 5\%$. The χ^2 analysis for the HK detector leads to $S_{\mathrm{lim}} = 9900$ at 90% C.L.

$$|g_{3aN} \times g_{ae}| \leq 1.22 \times 10^{-13} \quad \text{for } m_a \lesssim 1 \text{ MeV}, \tag{35}$$

at 90% C.L. Comparing this result with the sensitivity of JUNO, in Eq. (22), it can be concluded that JUNO can provide constraints about an order of magnitude more stringent than HK.

Similarly, we have investigated the HK sensitivity for the axion-photon and axion-nucleon couplings. In the small mass limit ($m_a \lesssim 10$ keV), solar axions would be detected via inverse Primakoff absorption on oxygen. Utilizing

Eq. (27), replacing N_C with the number of oxygen $N_O \simeq 1.25 \times 10^{34}$, the HK sensitivity at 90% C.L.reads

$$|g_{3aN} \times g_{a\gamma}| \lesssim 1.18 \times 10^{-11}\ \text{GeV}^{-1} \quad \text{for } m_a \lesssim 10\ \text{keV}. \quad (36)$$

Even in this case, we find that JUNO can explore couplings about an order of magnitude smaller than HK. Indeed, though its exposure is lower than HK, JUNO has better sensitivity due to its excellent energy resolution [Cf. Eqs. (7) and (32)].

Let us conclude by mentioning that the future Deep Underground Neutrino Experiment (DUNE) detector, which is currently under construction and expected to start taking data in the early-2030s, is less suitable to detect 5.49 MeV axions due to its high energy threshold ($E_{\text{th}} \gtrsim 5$ MeV) [132] and a higher background due to natural radioactivity in the surrounding rock and due to the charged current interaction of solar neutrinos on argon [133,134].

VI. CONCLUSIONS

In this work we have investigated the sensitivity of the neutrino detector JUNO to probe 5.49 MeV solar axions produced in the $p(d, {}^3\text{He})a$ reaction. The possible detection through Compton conversion would allow JUNO to probe the combination $|g_{3aN} \times g_{ae}| \gtrsim 6.33 \times 10^{-14}$ at 90% C.L. for $m_a \lesssim 1$ MeV. For larger masses, axions can decay into electron-positron pairs and the JUNO sensitivity reaches $|g_{3aN} \times g_{ae}| \sim 10^{-8}$. On the other hand, due to the inverse Primakoff process JUNO will explore the combination $|g_{3aN} \times g_{a\gamma}| \gtrsim 6.5 \times 10^{-12}$ GeV^{-1} for $m_a \lesssim 10$ keV, while for larger masses the axion decay into photons leads to the sensitivity $|g_{3aN} \times g_{a\gamma}| \times m_a^2 \lesssim 3.3 \times 10^{-12}$ eV.

Due to its large exposure time and the excellent energy resolution, JUNO will be able to set the strongest experimental limits on the combinations $|g_{3aN} \times g_{ae}|$ and $|g_{3aN} \times g_{a\gamma}|$, improving by more than one order of magnitude the Borexino bounds, and it has the best sensitivity among the current and proposed neutrino experiments, such as Hyper-Kamiokande.

Our study has shown an example of the physics potential of large underground neutrino detectors in probing axions. Other studies could include the evaluation of the Super-Kamiokande sensitivity to detect muonphilic axions produced from charged-meson decays in air showers [135] and the search for cosmogenic relativistic axions with future neutrino detectors, such as HK and JUNO itself [101]. This connection deserves further investigations to complement the standard experimental techniques to study axions.

ACKNOWLEDGMENTS

We warmly thank Eligio Lisi for helpful discussions and comments on the manuscript, as well as Davide Franco for clarifying some aspects of the Borexino analysis in the first stage of this work. The work of G. L. and A. M. is partially supported by the Italian Istituto Nazionale di Fisica Nucleare (INFN) through the "Theoretical Astroparticle Physics" project and by the research Grant No. 2017W4HA7S "NAT-NET: Neutrino and Astroparticle Theory Network" under the program PRIN 2017 funded by the Italian Ministero dell'Università e della Ricerca (MUR). N. N. is supported by the Istituto Nazionale di Fisica Nucleare (INFN) through the "Theoretical Astroparticle Physics" (TAsP) project.

APPENDIX: SUPERNOVA BOUND

In this Appendix, we present a short discussion of the SN bound on the axion-nucleon coupling g_{3aN}. In general, SN 1987A provides one of the most stringent bounds on the axion-nucleon couplings. Axions with mass up to $\lesssim$100 MeV, as the ones considered in this work, can be thermally produced in a SN and, if their couplings are sufficiently weak, they stream out without being reabsorbed. This, in turn, could dramatically alter the predictions for the observed neutrino signal from SN 1987A [136–138].

Here, we consider the most updated SN bound [115], which assumes the nucleon-nucleon bremsstrahlung production of axions, $NN \to NNa$.[11] We further assume that the axion-nucleon coupling is small enough to allow them to escape from the SN (free streaming regime). The exact free streaming threshold is quite difficult to calculate but we can assume $g_{3aN} \sim 10^{-6}$ [115].

The bound in Ref. [115] applies to a specific combination of the axion coupling to neutrons (g_{an}) and protons (g_{ap})

$$f(g_{an}, g_{ap}) < 8.26 \times 10^{-19},$$

where

$$f(g_{an}, g_{ap}) = g_{an}^2 + 0.61 g_{ap}^2 + 0.53 g_{an} g_{ap}.$$

To translate this bound into a constraint on g_{3aN}, we define $x = g_{ap}/g_{an}$ and express g_{an} in terms of the effective coupling $g_{3aN} = (g_{ap} - g_{an})/2 \Rightarrow g_{an} = 2g_{3aN}/(1 - x)$. So we get

[11] Refs. [139,140] showed that the production through scattering on negative pions would be more efficient production mechanism. However, no explicit bound was presented in this case. We will ignore this possibility here.

$$f = \frac{4g_{3aN}^2}{(1-x)^2}(1 + 0.53x + 0.61x^2).$$

The function f has a minimum for $x = -2.53/1.75$, corresponding to $f \simeq g_{3aN}^2$. Thus, we find

$$g_{3aN} < 9.1 \times 10^{-10}. \quad \text{(A1)}$$

This value represents the lower limit of the SN cooling bound on g_{3aN} shown as the pink region in Fig. 5 and Fig. 7.

[1] R. D. Peccei and H. R. Quinn, *CP* Conservation in the Presence of Instantons, Phys. Rev. Lett. **38**, 1440 (1977).
[2] F. Wilczek, Problem of Strong P and T Invariance in the Presence of Instantons, Phys. Rev. Lett. **40**, 279 (1978).
[3] S. Weinberg, A New Light Boson?, Phys. Rev. Lett. **40**, 223 (1978).
[4] M. Dine and W. Fischler, The not so harmless axion, Phys. Lett. **120B**, 137 (1983).
[5] L. F. Abbott and P. Sikivie, A cosmological bound on the invisible axion, Phys. Lett. **120B**, 133 (1983).
[6] J. Preskill, M. B. Wise, and F. Wilczek, Cosmology of the invisible axion, Phys. Lett. **120B**, 127 (1983).
[7] R. L. Davis, Cosmic axions from cosmic strings, Phys. Lett. B **180**, 225 (1986).
[8] J. E. Kim and G. Carosi, Axions and the strong *CP* problem, Rev. Mod. Phys. **82**, 557 (2010); Erratum, Rev. Mod. Phys. **91**, 049902 (2019).
[9] D. J. E. Marsh, Axion cosmology, Phys. Rep. **643**, 1 (2016).
[10] C. B. Adams *et al.*, Axion dark matter, in 2022 Snowmass Summer Study (2022), arXiv:2203.14923.
[11] M. Baryakhtar *et al.*, Dark matter in extreme astrophysical environments, in 2022 Snowmass Summer Study (2022), arXiv:2203.07984.
[12] L. Di Luzio, M. Giannotti, E. Nardi, and L. Visinelli, The landscape of QCD axion models, Phys. Rep. **870**, 1 (2020).
[13] P. Agrawal and K. Howe, Factoring the strong *CP* problem, J. High Energy Phys. 12 (2018) 029.
[14] M. Kamionkowski and J. March-Russell, Planck scale physics and the Peccei-Quinn mechanism, Phys. Lett. B **282**, 137 (1992).
[15] R. Holman, S. D. H. Hsu, T. W. Kephart, E. W. Kolb, R. Watkins, and L. M. Widrow, Solutions to the strong *CP* problem in a world with gravity, Phys. Lett. B **282**, 132 (1992).
[16] S. M. Barr and D. Seckel, Planck scale corrections to axion models, Phys. Rev. D **46**, 539 (1992).
[17] V. A. Rubakov, Grand unification and heavy axion, JETP Lett. **65**, 621 (1997).
[18] Z. Berezhiani, L. Gianfagna, and M. Giannotti, Strong *CP* problem and mirror world: The Weinberg-Wilczek axion revisited, Phys. Lett. B **500**, 286 (2001).
[19] A. Hook, S. Kumar, Z. Liu, and R. Sundrum, High Quality QCD Axion and the LHC, Phys. Rev. Lett. **124**, 221801 (2020).
[20] P. Svrcek and E. Witten, Axions in string theory, J. High Energy Phys. 06 (2006) 051.
[21] A. Arvanitaki, S. Dimopoulos, S. Dubovsky, N. Kaloper, and J. March-Russell, String axiverse, Phys. Rev. D **81**, 123530 (2010).
[22] M. Cicoli, M. Goodsell, and A. Ringwald, The type IIB string axiverse and its low-energy phenomenology, J. High Energy Phys. 10 (2012) 146.
[23] P. W. Graham, D. E. Kaplan, and S. Rajendran, Cosmological Relaxation of the Electroweak Scale, Phys. Rev. Lett. **115**, 221801 (2015).
[24] I. G. Irastorza and J. Redondo, New experimental approaches in the search for axion-like particles, Prog. Part. Nucl. Phys. **102**, 89 (2018).
[25] P. Di Vecchia, M. Giannotti, M. Lattanzi, and A. Lindner, Round table on axions and axion-like particles, Proc. Sci., Confinement2018 (**2019**) 034.
[26] P. Agrawal *et al.*, Feebly-interacting particles: FIPs 2020 workshop report, Eur. Phys. J. C **81**, 1015 (2021).
[27] P. Sikivie, Invisible axion search methods, Rev. Mod. Phys. **93**, 015004 (2021).
[28] M. Giannotti, Aspects of axions and ALPs phenomenology, in *10th Symposium on Large TPCs for Low-Energy Rare Event Detection* (2022), 5, arXiv:2205.06831.
[29] M. Giannotti, I. G. Irastorza, J. Redondo, A. Ringwald, and K. Saikawa, Stellar recipes for axion hunters, J. Cosmol. Astropart. Phys. 10 (2017) 010.
[30] L. Di Luzio, M. Fedele, M. Giannotti, F. Mescia, and E. Nardi, Stellar evolution confronts axion models, J. Cosmol. Astropart. Phys. 02 (**2022**) 035.
[31] M. Giannotti, Exciting times, Nat. Phys. **13**, 530 (2017).
[32] C. O'Hare, cajohare/axionlimits: Axionlimits. https://cajohare.github.io/AxionLimits/ (2020).
[33] G. G. Raffelt, Astrophysical axion bounds diminished by screening effects, Phys. Rev. D **33**, 897 (1986).
[34] G. G. Raffelt, Plasmon decay into low mass bosons in stars, Phys. Rev. D **37**, 1356 (1988).
[35] A. Caputo, A. J. Millar, and E. Vitagliano, Revisiting longitudinal plasmon-axion conversion in external magnetic fields, Phys. Rev. D **101**, 123004 (2020).
[36] C. A. J. O'Hare, A. Caputo, A. J. Millar, and E. Vitagliano, Axion helioscopes as solar magnetometers, Phys. Rev. D **102**, 043019 (2020).
[37] E. Guarini, P. Carenza, J. Galan, M. Giannotti, and A. Mirizzi, Production of axionlike particles from photon conversions in large-scale solar magnetic fields, Phys. Rev. D **102**, 123024 (2020).
[38] J. Redondo, Solar axion flux from the axion-electron coupling, J. Cosmol. Astropart. Phys. 12 (2013) 008.

[39] S. Hoof, J. Jaeckel, and L. J. Thormaehlen, Quantifying uncertainties in the solar axion flux and their impact on determining axion model parameters, J. Cosmol. Astropart. Phys. 09 (2021) 006.
[40] V. Anastassopoulos *et al.* (CAST Collaboration), New CAST limit on the axion-photon interaction, Nat. Phys. **13**, 584 (2017).
[41] A. Ayala, I. Domínguez, M. Giannotti, A. Mirizzi, and O. Straniero, Revisiting the Bound on Axion-Photon Coupling from Globular Clusters, Phys. Rev. Lett. **113**, 191302 (2014).
[42] O. Straniero, A. Ayala, M. Giannotti, A. Mirizzi, and I. Dominguez, Axion-photon coupling: Astrophysical constraints, in *11th Patras Workshop on Axions, WIMPs and WISPs* (2015), pp. 77–81, http://dx.doi.org/10.3204/DESY-PROC-2015-02/straniero-oscar.
[43] M. J. Dolan, F. J. Hiskens, and R. R. Volkas, Advancing globular cluster constraints on the axion-photon coupling, J. Cosmol. Astropart. Phys. 10 (2022) 096.
[44] D. Wouters and P. Brun, Constraints on axion-like particles from x-ray observations of the hydra galaxy cluster, Astrophys. J. **772**, 44 (2013).
[45] M. C. D. Marsh, H. R. Russell, A. C. Fabian, B. P. McNamara, P. Nulsen, and C. S. Reynolds, A new bound on axion-like particles, J. Cosmol. Astropart. Phys. 12 (2017) 036.
[46] C. S. Reynolds, M. C. D. Marsh, H. R. Russell, A. C. Fabian, R. Smith, F. Tombesi, and S. Veilleux, Astrophysical limits on very light axion-like particles from Chandra grating spectroscopy of NGC 1275, Astrophys. J. **890**, 59 (2020).
[47] C. Dessert, J. W. Foster, and B. R. Safdi, X-Ray Searches for Axions from Super Star Clusters, Phys. Rev. Lett. **125**, 261102 (2020).
[48] M. Xiao, K. M. Perez, M. Giannotti, O. Straniero, A. Mirizzi, B. W. Grefenstette, B. M. Roach, and M. Nynka, Constraints on Axionlike Particles from a Hard X-Ray Observation of Betelgeuse, Phys. Rev. Lett. **126**, 031101 (2021).
[49] J. S. Reynés, J. H. Matthews, C. S. Reynolds, H. R. Russell, R. N. Smith, and M. C. D. Marsh, New constraints on light axion-like particles using Chandra transmission grating spectroscopy of the powerful cluster-hosted quasar H1821 + 643, Mon. Not. R. Astron. Soc. **510**, 1264 (2021).
[50] F. Calore, P. Carenza, C. Eckner, T. Fischer, M. Giannotti, J. Jaeckel, K. Kotake, T. Kuroda, A. Mirizzi, and F. Sivo, 3D template-based Fermi-LAT constraints on the diffuse supernova axion-like particle background, Phys. Rev. D **105**, 063028 (2022).
[51] C. Dessert, A. J. Long, and B. R. Safdi, No Evidence for Axions from Chandra Observation of the Magnetic White Dwarf RE J0317-853, Phys. Rev. Lett. **128**, 071102 (2022).
[52] M. Xiao, P. Carenza, M. Giannotti, A. Mirizzi, K. M. Perez, O. Straniero, and B. W. Grefenstette, Betelgeuse constraints on coupling between axion-like particles and electrons, arXiv:2204.03121.
[53] Y. Kahn, B. R. Safdi, and J. Thaler, Broadband and Resonant Approaches to Axion Dark Matter Detection, Phys. Rev. Lett. **117**, 141801 (2016).
[54] F. A. Harrison *et al.* (NuSTAR Collaboration), The nuclear spectroscopic telescope array (NuSTAR) high-energy X-ray mission, Astrophys. J. **770**, 103 (2013).
[55] W. DeRocco, S. Wegsman, B. Grefenstette, J. Huang, and K. Van Tilburg, First indirect detection constraints on axions in the Solar basin, Phys. Rev. Lett. **129**, 101101 (2022).
[56] E. Armengaud *et al.* (IAXO Collaboration), Physics potential of the International Axion Observatory (IAXO), J. Cosmol. Astropart. Phys. 06 (2019) 047.
[57] A. Abeln *et al.* (IAXO Collaboration), Conceptual design of BabyIAXO, the intermediate stage towards the International Axion Observatory, J. High Energy Phys. 05 (2021) 137.
[58] E. Aprile *et al.* (XENON Collaboration), Excess electronic recoil events in XENON1T, Phys. Rev. D **102**, 072004 (2020).
[59] D. S. Akerib *et al.* (LUX Collaboration), First Searches for Axions and Axionlike Particles with the LUX Experiment, Phys. Rev. Lett. **118**, 261301 (2017).
[60] C. Fu *et al.* (PandaX Collaboration), Limits on Axion Couplings from the First 80 Days of Data of the PandaX-II Experiment, Phys. Rev. Lett. **119**, 181806 (2017).
[61] O. Straniero, C. Pallanca, E. Dalessandro, I. Dominguez, F. R. Ferraro, M. Giannotti, A. Mirizzi, and L. Piersanti, The RGB tip of galactic globular clusters and the revision of the axion-electron coupling bound, Astron. Astrophys. **644**, A166 (2020).
[62] F. Capozzi and G. Raffelt, Axion and neutrino bounds improved with new calibrations of the tip of the red-giant branch using geometric distance determinations, Phys. Rev. D **102**, 083007 (2020).
[63] T. W. Donnelly, S. J. Freedman, R. S. Lytel, R. D. Peccei, and M. Schwartz, Do axions exist?, Phys. Rev. D **18**, 1607 (1978).
[64] G. Raffelt and L. Stodolsky, New particles from nuclear reactions in the sun, Phys. Lett. **119B**, 323 (1982).
[65] S. Moriyama, A Proposal to Search for a Monochromatic Component of Solar Axions Using Fe-57, Phys. Rev. Lett. **75**, 3222 (1995).
[66] M. Krcmar, Z. Krecak, M. Stipcevic, A. Ljubicic, and D. A. Bradley, Search for invisible axions using Fe-57, Phys. Lett. B **442**, 38 (1998).
[67] S. Andriamonje *et al.* (CAST Collaboration), Search for 14.4-keV solar axions emitted in the M1-transition of Fe-57 nuclei with CAST, J. Cosmol. Astropart. Phys. 12 (2009) 002.
[68] F. Alessandria *et al.* (CUORE Collaboration), Search for 14.4 keV solar axions from M1 transition of Fe-57 with CUORE crystals, J. Cosmol. Astropart. Phys. 05 (2013) 007.
[69] A. V. Derbin, A. I. Egorov, I. A. Mitropolsky, and V. N. Muratova, Search for solar axions emitted in an M1 transition in Li-7 nuclei, JETP Lett. **81**, 365 (2005).
[70] P. Belli *et al.*, Li-7 solar axions: Preliminary results and feasibility studies, Nucl. Phys. **A806**, 388 (2008).

[71] G. Bellini *et al.* (Borexino Collaboration), Search for solar axions emitted in the M1-transition of Li-7* with Borexino CTF, Eur. Phys. J. C **54**, 61 (2008).

[72] S. Andriamonje *et al.* (CAST Collaboration), Search for solar axion emission from ^{7}Li and $D(p,\gamma)^{3}$He nuclear decays with the CAST γ-ray calorimeter, J. Cosmol. Astropart. Phys. 03 (2010) 032.

[73] Y. M. Gavrilyuk *et al.*, First result of the experimental search for the 9.4 keV solar axion reactions with ^{83}Kr in the copper proportional counter, Phys. Part. Nucl. **46**, 152 (2015).

[74] K. Jakovcic, Z. Krecak, M. Krcmar, and A. Ljubicic, A Search for solar hadronic axions using ^{83}Kr, Radiat. Phys. Chem. **71**, 793 (2004).

[75] L. Di Luzio *et al.*, Probing the axion–nucleon coupling with the next generation of axion helioscopes, Eur. Phys. J. C **82**, 120 (2022).

[76] A. Bhusal, N. Houston, and T. Li, Searching for Solar Axions Using Data from the Sudbury Neutrino Observatory, Phys. Rev. Lett. **126**, 091601 (2021).

[77] G. Bellini *et al.* (Borexino Collaboration), Search for solar axions produced in $p(d,{}^{3}\mathrm{He})A$ reaction with borexino detector, Phys. Rev. D **85**, 092003 (2012).

[78] M. Agostini *et al.* (Borexino Collaboration), Improved measurement of ^{8}B solar neutrinos with 1.5 $kt \cdot y$ of Borexino exposure, Phys. Rev. D **101**, 062001 (2020).

[79] K. Abe *et al.* (Super-Kamiokande Collaboration), Solar neutrino measurements in Super-Kamiokande-IV, Phys. Rev. D **94**, 052010 (2016).

[80] F. An *et al.* (JUNO Collaboration), Neutrino physics with JUNO, J. Phys. G **43**, 030401 (2016).

[81] A. Abusleme *et al.* (JUNO Collaboration), Feasibility and physics potential of detecting ^{8}B solar neutrinos at JUNO, Chin. Phys. C **45**, 023004 (2021).

[82] J. D. Vergados, P. C. Divari, and H. Ejiri, Calculated event rates for axion detection via atomic and nuclear processes, Adv. High Energy Phys. **2022**, 7373365 (2022).

[83] R. Massarczyk, P. H. Chu, and S. R. Elliott, Axion emission from nuclear magnetic dipole transitions, Phys. Rev. D **105**, 015031 (2022).

[84] F. T. Avignone, C. Baktash, W. C. Barker, F. P. Calaprice, R. W. Dunford, W. C. Haxton, D. Kahana, R. T. Kouzes, H. S. Miley, and D. M. Moltz, Search for Axions from the 1115-kev transition of ^{65}Cu, Phys. Rev. D **37**, 618 (1988).

[85] A. M. Serenelli, W. C. Haxton, and C. Pena-Garay, Solar models with accretion. I. Application to the solar abundance problem, Astrophys. J. **743**, 24 (2011).

[86] M. Agostini *et al.* (Borexino Collaboration), First simultaneous precision spectroscopy of pp, ^{7}Be, and pep solar neutrinos with Borexino Phase-II, Phys. Rev. D **100**, 082004 (2019).

[87] A. Abusleme *et al.* (JUNO Collaboration), Prospects for detecting the diffuse supernova neutrino background with JUNO, J. Cosmol. Astropart. Phys. 10 (2022) 033.

[88] K. O. Mikaelian, Astrophysical implications of new light Higgs bosons, Phys. Rev. D **18**, 3605 (1978).

[89] S. J. Brodsky, E. Mottola, I. J. Muzinich, and M. Soldate, Laser Induced Axion Photoproduction, Phys. Rev. Lett. **56**, 1763 (1986); Erratum, Phys. Rev. Lett. **57**, 502 (1986).

[90] R. Chanda, J. F. Nieves, and P. B. Pal, Astrophysical constraints on axion and Majoron couplings, Phys. Rev. D **37**, 2714 (1988).

[91] S. Dimopoulos, G. D. Starkman, and B. W. Lynn, Atomic enhancements in the detection of axions, Mod. Phys. Lett. A **01**, 491 (1986).

[92] M. Pospelov, A. Ritz, and M. B. Voloshin, Bosonic super-WIMPs as keV-scale dark matter, Phys. Rev. D **78**, 115012 (2008).

[93] A. Derevianko, V. A. Dzuba, V. V. Flambaum, and M. Pospelov, Axio-electric effect, Phys. Rev. D **82**, 065006 (2010).

[94] B. R. Kim, R. Rodenberg, and C. Stamm, Lepton pair production of a light pseudoscalar particle via the Bethe-Heitler process, Phys. Lett. **122B**, 87 (1983).

[95] B. R. Kim, B. H. Cho, S. K. Oh, C. Stamm, and R. Rodenberg, A numerical formula for the total cross-section of the lepton pair production via the Bethe-Heitler process of a light pseudoscalar particle, Nucl. Phys. **B242**, 189 (1984).

[96] J. Blumlein *et al.*, Limits on the mass of light (pseudo) scalar particles from Bethe-Heitler e + e− and mu + mu− pair production in a proton—iron beam dump experiment, Int. J. Mod. Phys. A **07**, 3835 (1992).

[97] A. R. Zhitnitsky and Y. I. Skovpen, On production and detecting of axions at penetration of electrons through matter (in Russian), Sov. J. Nucl. Phys. **29**, 513 (1979); [Yad. Fiz. **29**, 995 (1979).]

[98] M. Berger, J. Hubbell, S. Seltzer, J. Chang, J. Coursey, R. Sukumar, D. Zucker, and K. Olsen, Xcom: Photon cross sections database, https://www.nist.gov/pml/xcom-photon-cross-sections-database.

[99] W. A. Bardeen, S. H. H. Tye, and J. A. M. Vermaseren, Phenomenology of the new light Higgs boson search, Phys. Lett. **76B**, 580 (1978).

[100] V. Brdar, B. Dutta, W. Jang, D. Kim, I. M. Shoemaker, Z. Tabrizi, A. Thompson, and J. Yu, Axionlike Particles at Future Neutrino Experiments: Closing the Cosmological Triangle, Phys. Rev. Lett. **126**, 201801 (2021).

[101] Y. Cui, J.-L. Kuo, J. Pradler, and Y.-D. Tsai, Shining light on cosmogenic axions with neutrino experiments, arXiv:2207.13107.

[102] K. J. Kim and Y.-S. Tsai, Improved Weizsacker-Williams method and its application to lepton and w boson pair production, Phys. Rev. D **8**, 3109 (1973).

[103] Y.-S. Tsai, Pair Production, and Bremsstrahlung of charged leptons, Rev. Mod. Phys. **46**, 815 (1974); Erratum, Rev. Mod. Phys. **49**, 421 (1977).

[104] A. Abusleme *et al.* (JUNO Collaboration), JUNO physics and detector, Prog. Part. Nucl. Phys. **123**, 103927 (2022).

[105] S. Baker and R. D. Cousins, Clarification of the use of chi square and likelihood functions in fits to histograms, Nucl. Instrum. Methods **221**, 437 (1984).

[106] A. V. Derbin, S. V. Bakhlanov, I. S. Dratchnev, A. S. Kayunov, and V. N. Muratova, Search for axioelectric effect of 5.5 MeV solar axions using BGO detectors, Eur. Phys. J. C **73**, 2490 (2013).

[107] A. V. Derbin *et al.*, Search for axioelectric effect of solar axions using BGO scintillating bolometer, Eur. Phys. J. C **74**, 3035 (2014).

[108] H. M. Chang *et al.* (TEXONO Collaboration), Search of axions at the Kuo-Sheng nuclear power station with a high-purity germanium detector, Phys. Rev. D **75**, 052004 (2007).
[109] D. Aristizabal Sierra, V. De Romeri, L. J. Flores, and D. K. Papoulias, Axionlike particles searches in reactor experiments, J. High Energy Phys. 03 (2021) 294.
[110] L. Waites, A. Thompson, A. Bungau, J. M. Conrad, B. Dutta, W.-C. Huang, D. Kim, M. Shaevitz, and J. Spitz, Axion-like particle production at beam dump experiments with distinct nuclear excitation lines,
[111] E. Armengaud *et al.* (EDELWEISS Collaboration), Searches for electron interactions induced by new physics in the EDELWEISS-III Germanium bolometers, Phys. Rev. D **98**, 082004 (2018).
[112] S. K. Liu *et al.* (CDEX Collaboration), Constraints on Axion couplings from the CDEX-1 experiment at the China Jinping Underground Laboratory, Phys. Rev. D **95**, 052006 (2017).
[113] N. Abgrall *et al.* (Majorana Collaboration), New limits on Bosonic Dark Matter, Solar Axions, Pauli Exclusion Principle Violation, and Electron Decay from the Majorana Demonstrator, Phys. Rev. Lett. **118**, 161801 (2017).
[114] C. Fu *et al.* (PandaX Collaboration), Limits on Axion Couplings from the First 80 Days of Data of the PandaX-II Experiment, Phys. Rev. Lett. **119**, 181806 (2017).
[115] P. Carenza, T. Fischer, M. Giannotti, G. Guo, G. Martínez-Pinedo, and A. Mirizzi, Improved axion emissivity from a supernova via nucleon-nucleon bremsstrahlung, J. Cosmol. Astropart. Phys. 10 (2019) 016.
[116] M. Dine, W. Fischler, and M. Srednicki, A simple solution to the strong *CP* problem with a harmless axion, Phys. Lett. **104B**, 199 (1981).
[117] A. R. Zhitnitsky, On possible suppression of the axion hadron interactions (In Russian), Sov. J. Nucl. Phys. **31**, 260 (1980); [Yad. Fiz. **31**, 497 (1980).]
[118] G. Lucente and P. Carenza, Supernova bound on axionlike particles coupled with electrons, Phys. Rev. D **104**, 103007 (2021).
[119] R. Z. Ferreira, M. C. D. Marsh, and E. Müller, Strong supernovae bounds on ALPs from quantum loops, arXiv:2205.07896.
[120] J. Engel, D. Seckel, and A. C. Hayes, Emission and Detectability of Hadronic Axions from SN1987A, Phys. Rev. Lett. **65**, 960 (1990).
[121] A. Caputo, G. Raffelt, and E. Vitagliano, Muonic boson limits: Supernova redux, Phys. Rev. D **105**, 035022 (2022).
[122] P. Carenza, O. Straniero, B. Döbrich, M. Giannotti, G. Lucente, and A. Mirizzi, Constraints on the coupling with photons of heavy axion-like-particles from Globular Clusters, Phys. Lett. B **809**, 135709 (2020).
[123] G. Lucente, O. Straniero, P. Carenza, M. Giannotti, and A. Mirizzi, Constraining Heavy Axionlike Particles by Energy Deposition in Globular Cluster Stars, Phys. Rev. Lett. **129**, 011101 (2022).
[124] M. J. Dolan, T. Ferber, C. Hearty, F. Kahlhoefer, and K. Schmidt-Hoberg, Revised constraints and Belle II sensitivity for visible and invisible axion-like particles, J. High Energy Phys. 12 (2017) 094.
[125] B. Döbrich, J. Jaeckel, and T. Spadaro, Light in the beam dump—ALP production from decay photons in proton beam-dumps, J. High Energy Phys. 05 (2019) 213; Erratum, J. High Energy Phys. 10 (2020) 46.
[126] A. Caputo, H.-T. Janka, G. Raffelt, and E. Vitagliano, Low-Energy Supernovae Severely Constrain Radiative Particle Decays, Phys. Rev. Lett. **128**, 221103 (2022).
[127] J. Jaeckel, P. C. Malta, and J. Redondo, Decay photons from the axionlike particles burst of type II supernovae, Phys. Rev. D **98**, 055032 (2018).
[128] K. Abe *et al.* (Hyper-Kamiokande Collaboration), Hyper-Kamiokande Design Report, arXiv:1805.04163.
[129] E. O'Sullivan, The Hyper-Kamiokande Experiment (2019), https://indico.cern.ch/event/813935/contributions/3558094/attachments/1918804/3173545/eosullivan_partikeldagarna2019.pdf.
[130] J. N. Bahcall, E. Lisi, D. E. Alburger, L. De Braeckeleer, S. J. Freedman, and J. Napolitano, Standard neutrino spectrum from B-8 decay, Phys. Rev. C **54**, 411 (1996).
[131] C. Giunti and C. W. Kim, *Fundamentals of Neutrino Physics and Astrophysics* (Oxford University Press, 2007).
[132] B. Abi *et al.* (DUNE Collaboration), Deep underground neutrino experiment (DUNE), far detector technical design report, Volume II: DUNE Physics, arXiv:2002.03005.
[133] F. Capozzi, S. W. Li, G. Zhu, and J. F. Beacom, DUNE as the Next-Generation Solar Neutrino Experiment, Phys. Rev. Lett. **123**, 131803 (2019).
[134] G. Zhu, S. W. Li, and J. F. Beacom, Developing the MeV potential of DUNE: Detailed considerations of muon-induced spallation and other backgrounds, Phys. Rev. C **99**, 055810 (2019).
[135] K. Cheung, J.-L. Kuo, P.-Y. Tseng, and Z. S. Wang, Atmospheric axion-like particles at Super-Kamiokande, Phys. Rev. D **106**, 095029 (2022).
[136] G. Raffelt and D. Seckel, Bounds on Exotic Particle Interactions from SN 1987a, Phys. Rev. Lett. **60**, 1793 (1988).
[137] M. S. Turner, Axions from SN 1987a, Phys. Rev. Lett. **60**, 1797 (1988).
[138] R. Mayle, J. R. Wilson, J. R. Ellis, K. A. Olive, D. N. Schramm, and G. Steigman, Constraints on axions from SN 1987a, Phys. Lett. B **203**, 188 (1988).
[139] P. Carenza, B. Fore, M. Giannotti, A. Mirizzi, and S. Reddy, Enhanced Supernova Axion Emission and its Implications, Phys. Rev. Lett. **126**, 071102 (2021).
[140] T. Fischer, P. Carenza, B. Fore, M. Giannotti, A. Mirizzi, and S. Reddy, Observable signatures of enhanced axion emission from protoneutron stars, Phys. Rev. D **104**, 103012 (2021).